

STUDY OF AN UNSATURATED SLOPE FAILURE DUE TO RAINFALL INFILTRATION IN WENSHAN DISTRICT OF TAIPEI CITY

Horn-Da Lin¹, Jhih-Rou Huang^{2*}, Wei-Chien Wang³, and Chao-Wei Chen⁴

ABSTRACT

Traditionally, the analysis of the rainfall-induced slope failure was assumed to be under saturated condition. Nevertheless, lots of colluvium slopes are unsaturated in the normal condition in Taiwan. Unsaturated slopes have matric suction, contributing to their high slope stabilities in the dry season. With the rainfall infiltration, the decrease of matric suction may lead to the failure of the slope. This paper presents the numerical analysis of a case located in Wenshan Dist., Taipei City, Taiwan. The slope collapsed during Typhoon Jangmi in September 2008. Since the remediation program was urgent then, there was not enough time to comprehensively figure out the failure mechanism of the case. Consequently, this study conducts the site investigation and performs the numerical analysis to better understand the real failure mechanism of this slope. Results reveal that the failure is shallow and progressive. Additionally, the toe of colluvium was the most susceptible part of the whole slope during infiltration. Furthermore, the critical volumetric water content existed, when the slope collapsed. Accordingly, the monitoring system ought to be set in the toe of the colluvium and the volumetric water content may be considered as an index parameter for the early warning system of landslide disasters in the future..

Key words: Unsaturated soil; rainfall infiltration; hydrological responses; slope stability; colluvium.

1. INTRODUCTION

With climate change, Taiwan receives abundant rainfall annually. Furthermore, Taiwan is on the Pacific Ring of Fire, seismically active zone. Due to the weak geology, typhoons and heavy rainfall contribute to catastrophic disasters such as landslides, floods and so on (Shou *et al.* 2018; Wu *et al.* 2016). In specific, the rainfall-induced slope failure is a major geotechnical disaster in Taiwan.

Lots of slopes are mainly composed of colluvium in Taiwan (Lee *et al.* 2013; Lo *et al.* 2011). Rainfall-induced shallow slope failures are common in colluvium (Chung *et al.* 2018; Jeng *et al.* 2013; Lin *et al.* 2010; Yang *et al.* 2016). Studies indicate that failure surfaces of colluvium slopes usually located above the groundwater tables which do not change significantly subject to infiltration (Collins and Znidarcic 2004; Gerscovich *et al.* 2006; Kim *et al.* 2004).

Conventionally, the variation of the groundwater table was assumed to be the main effect of rainfall on the slope in the analyses. Nonetheless, this method only considers the saturated portion of the slope below the groundwater table. Hence, the influ-

Manuscript received December 25, 2018; revised May 19, 2019; accepted July 25, 2019.

¹ Professor, Department of Civil and Construction Engineering, National Taiwan University of Science and Technology, Taipei, Taiwan 10607, R.O.C.

^{2*} Research Assistant (corresponding author), Department of Civil and Construction Engineering, National Taiwan University of Science and Technology, Taipei, Taiwan 10607, R.O.C. (e-mail: b10305003@mail.ntust.edu.tw).

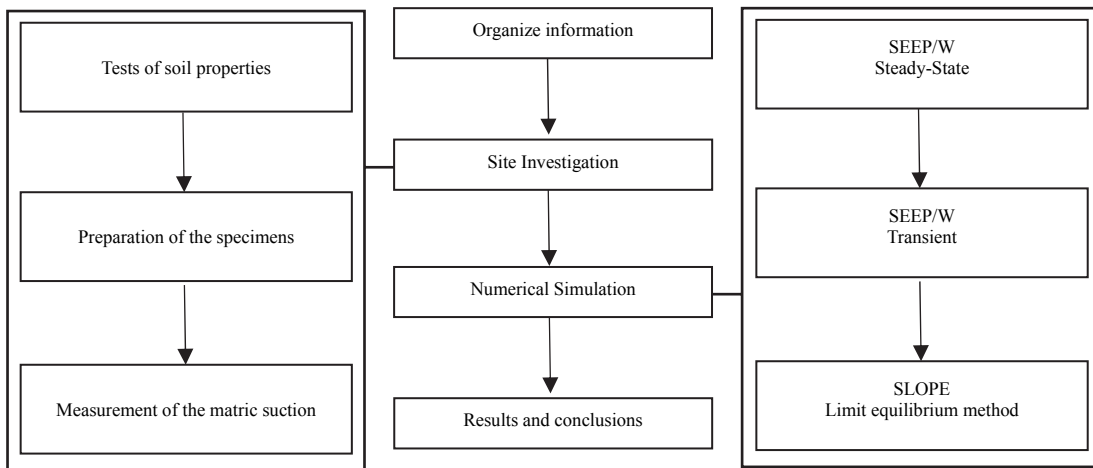
³ Ph.D. Candidate, Department of Civil and Construction Engineering, National Taiwan University of Science and Technology, Taipei, Taiwan 10607, R.O.C.

⁴ General Manager, Land Engineering Consultants Co., Ltd.

ence regarding rainfall infiltration on the unsaturated part of the slope may be ignored, leading to incorrect evaluations and possible misinterpretation of the failure mechanism of the slope.

In fact, the development of rainfall-induced wetting front is the primary failure mechanism resulting in the decrease of suction and shear strength of soil (Kim *et al.* 2004; Yang *et al.* 2008). Additionally, studies show that hydrological responses of unsaturated soil change simultaneously with the wetting and drying cycles during rainfall (Gui *et al.* 2014; Montoya- Domínguez *et al.* 2016; Urciuoli *et al.* 2016). Apparently, hydrological responses reveal the stability of slope directly (Chen *et al.* 2012). Therefore, the estimation of hydrological responses for unsaturated slopes under infiltration is essential (Cho 2014; Cho 2016; Chung *et al.* 2018; Huang *et al.* 2013; Lee *et al.* 2016). This study pertains to a case in which an urgent remediation program was required, so there was no time to fully understand the failure mechanism of the case then. The real failure mechanism for this case is in question. Therefore, hydrological responses that give the useful index to landslides may be helpful to figure out the failure mechanism. The comprehensive numerical analysis was conducted to study this case. The research flowchart is shown in Fig. 1.

This paper studies the unstable slope (Lin *et al.* 2018) in Wenshan District of Taipei City. Since the thickness of the colluvium is non-uniform in the case, the hydrological response of this slope is not similar to the uniform one. Except for trying to find out the real failure mechanism of the slope, the paper derives the relationship between the hydrological response and the stability of unsaturated slopes during rainfall for this kind of slope. Additionally, the volumetric water content is recommended to be monitored in the lower part of colluvium which is the most sensitive portion of the entire slope subject to the rainfall infiltration to predict landslide disasters.

**Fig. 1** Research flowchart

2. CASE HISTORY

The slope is composed of colluvium and the groundwater table locates deeply below the bottom of the colluvium in this case. Accordingly, the failure mechanism of this slope could be assumed to be a shallow collapse. To understand the effect of the infiltration on the unsaturated part of the slope, this study performs the numerical analysis to better understand the real failure mechanism for this unstable slope.

2.1 Landslide Event

The unstable slope is situated on Xinguang Rd., Wenshan Dist., Taipei City, Taiwan (Fig. 2). The slope collapsed during Typhoon Jangmi which passed over Taiwan on September 26–29,

2008. The meteorological record shows that the total precipitation during Typhoon Jangmi was roughly 453 mm in 4 days. A private house and a chicken coop were buried in the collapse, contributing to the loss of thousands of poultry. Traffic movements in the region were also suspended because of the concern for safety. Fig. 3 displays the condition of the slope after the collapse. As a result, an urgent remediation program was implemented to ensure the stability of the slope.

In this case, the slope slid from southwest to northeast. The landslide area was 100 ~ 120 m wide and 100 ~ 150 m long. The total sliding area was approximately 1 ~ 2 ha. Furthermore, the landslide area is at the elevation of 180 ~ 240 m above sea level (Land Engineering Consultants Co., Ltd. 2008).

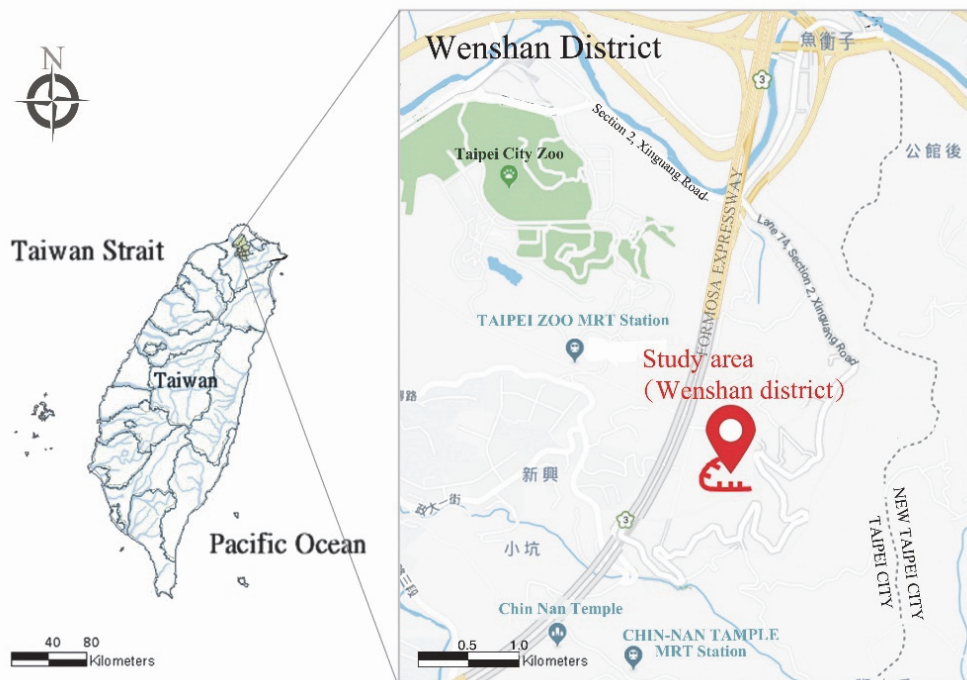
**Fig. 2** Location of study area in Taipei City (Google map)



Fig. 3 The condition of the slope after the collapse (Land Engineering Consultants Co., Ltd. 2008)

3. SITE INVESTIGATION

Colluvium is the most susceptible part of the entire slope subject to rainfall infiltration. Based on monitoring results, the groundwater table in this slope varied in the range of 25 ~ 45 m below the bottom of colluvium (Land Engineering Consultants Co., Ltd. 2008). In other words, the colluvium is unsaturated and above the groundwater table under normal conditions. Furthermore, the soil water characteristic curve (SWCC) is essential to determine the permeability. Accordingly, the pressure plate test was conducted on the colluvium to ensure the accuracy of the parameters for the numerical analysis.

3.1 Test Program

Soil samples for this study were taken from the slope in the Wenshan district of Taipei. To make specimens for the pressure plate test, several laboratory tests were conducted on the samples. Soil specimens were made according to in-situ properties such as density and water content. Moreover, static compaction was used

in this study to remold the samples, in order to ensure that the initial condition of the specimens was homogeneous. Basic soil properties, the procedures for sample preparation and the test are discussed further in the following.

3.2 Soil Properties

The basic physical properties of these samples are summarized in Table. 1. The specific gravity and the Atterberg limits for this study were conducted according to ASTM D854-83 and ASTM D4318-10, separately. Additionally, the grain size distribution tests were done in accordance with ASTM D452-85. Two sets of soil samples are classified as CL (clay of low plasticity, sample A) and SC (clayey sand, sample B) respectively based on the Unified Soil Classification System (Fig. 4). In the results of X-Ray Diffraction (XRD) tests, sample A has 67% Illite and 10% quartz for the mineral composition. Sample B has 66% Illite and 18% Quartz for the mineral composition. That is to say, the principal minerals in these samples are similar which are Illite and Quartz (Fig. 5).

Table 1 Soil properties

	G_s	LL (%)	PL (%)	PI (%)	Gravel (%) ($> \#4$)	Silt & Clay (%) ($< \#200$)
Sample A (CL)	2.59	34.7	21.1	13.6	0	70.3
Sample B (SC)	2.58	44.2	22.4	21.8	12.6	18.6



(a) Sample A



(b) Sample B

Fig. 4 Soil samples

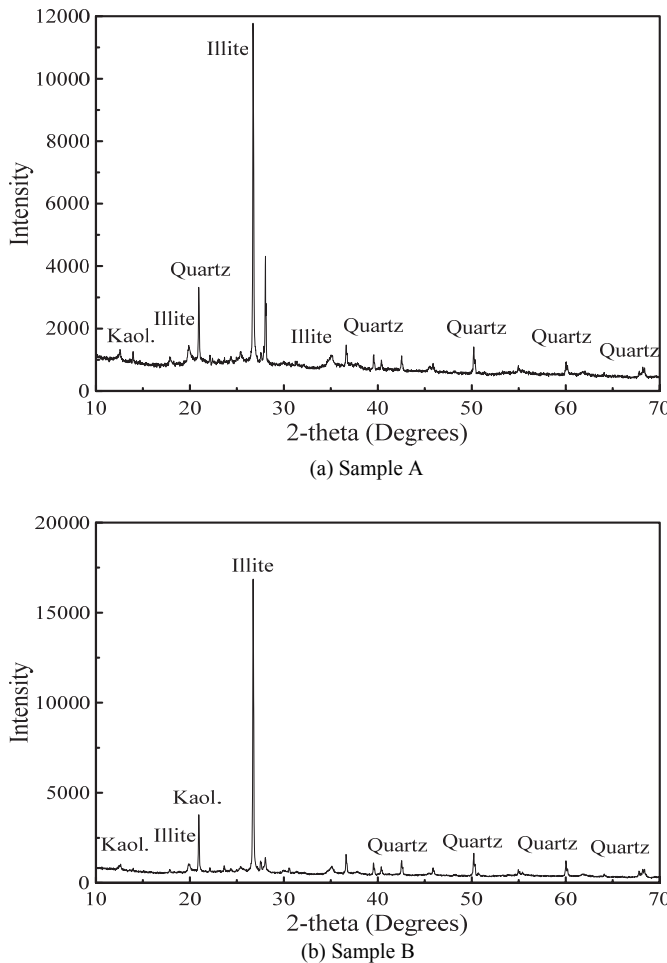


Fig. 5 Mineral composition of samples

3.3 Preparation of the Specimens

The dry density and water content of the soils were measured using sand-cone tests to ASTM D1556 (Fig. 6). Thereafter, with a view to ensuring the uniform water contents of samples, the well-mixed soils were stored in zipper bags for 24 hours. The soils were then transferred to the mold and compacted by static pressure into a remolded specimen. The samples were 2 cm in height, and 5 cm in diameter. The weight of the mold was about 20 g.

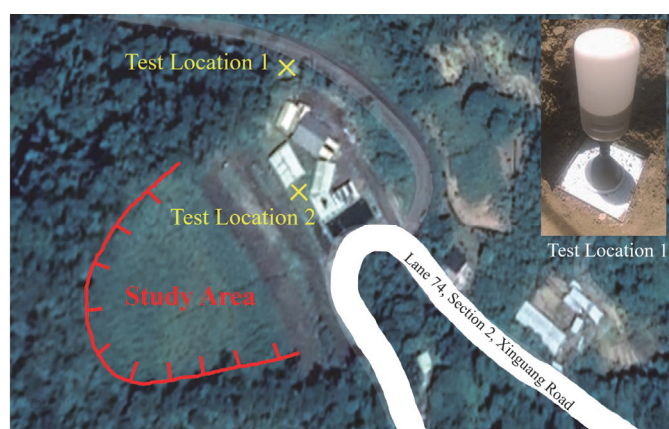


Fig. 6 Locations of sand-cone test (Google map)

3.4 Measurement of the Matric Suction

The pressure plate test adheres to the ASTM D3152-72 standard to obtain the Soil-Water Characteristic Curve (SWCC). The pressure plate extractor of 500 kPa used in this study was made by Soilmoisture Equipment Corp (Fig. 7). It consists of a pressure vessel that is pressurized by nitrogen to a pressure of 500 kPa.

The specimens were saturated in the oedometer for 2 ~ 3 days using the contact stress of 2.5 kPa as defined by ASTM D2345-80. Afterward, samples were put into the extractor for the pressure plate test. During the test, the pressure was applied in steps at 10kPa, 20 kPa, 40kPa, 80kPa, 100kPa, and 200kPa separately. To determine the state of equilibrium, the samples were weighed every 24 hr for each pressure step. The test results show that the SWCCs for these two samples are similar in shape and the air entry value are about 40 ~ 50 kPa (Fig. 8). Moreover, the X-Ray Diffraction (XRD) test results show that these two samples have a similar mineral composition (Fig. 5). Thus, this shape of SWCC (red line in Fig. 8) was used with the volumetric water content that was measured in the field to do the analysis.



Fig. 7 Pressure plate equipment

4. NUMERICAL SIMULATION

When the properties of colluvium have been determined, Geo-Studio is used for the numerical analysis for this study.

4.1 Numerical Procedures

The initial boundary condition is set in SEEP/W for a steady seepage analysis. The recorded rainfall data is then inputted for the transient seepage analysis. For SEEP/W, Eq. (1) for transient flow is derived from the study by Richards (1931).

$$K_x \frac{\partial^2 H}{\partial x^2} + K_y \frac{\partial^2 H}{\partial y^2} = \frac{\partial \theta}{\partial t} \quad (1)$$

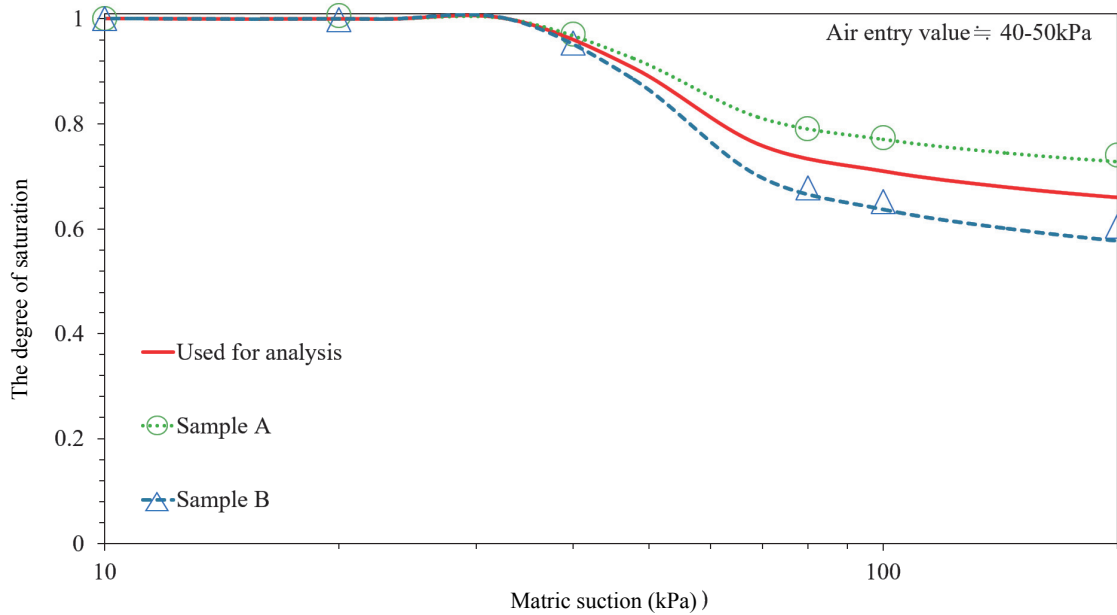


Fig. 8 Soil water characteristic curves (SWCCs) of colluvium

where H is the total hydraulic head of flow; k_x and k_y respectively represent the hydraulic conductivities in the x -direction and the y -direction; θ is the volumetric water content and t is time.

In this study, the soil water characteristic curve is obtained from the pressure plate test. The hydraulic conductivity curve (Fig. 9) is estimated using the saturated hydraulic conductivity and three curve fitting parameters (Van Genuchten 1980). The curve fitting parameters in Eq. (2) are calculated using the soil water characteristic curve. The k -function curve is derived from Eq. (2), Eq. (3), and Fig. 8. The k -curves for these two samples are shown in Fig. 9. Since the curves for sample A and sample B are close to each other, the red line (Fig. 9) is used in the analysis.

$$\theta = \theta_r + \frac{\theta_s - \theta_r}{\left[1 + \left(\frac{\Psi}{a}\right)^n\right]^m} \quad (2)$$

$$k = k_s + \frac{[1 - (a\Psi^{n-1})(1 + a\Psi^n)^{-m}]^{\frac{m}{n}}}{(1 + (a\Psi)^n)^2} \quad (3)$$

where θ is the volumetric water content; θ_s is the saturated volumetric water content; θ_r is the residual volumetric water content; Ψ is the negative pore-water pressure; a , n , m are the curve fitting parameters and $n = 1/(1 - m)$; k is the hydraulic conductivity; k_s is the saturated hydraulic conductivity.

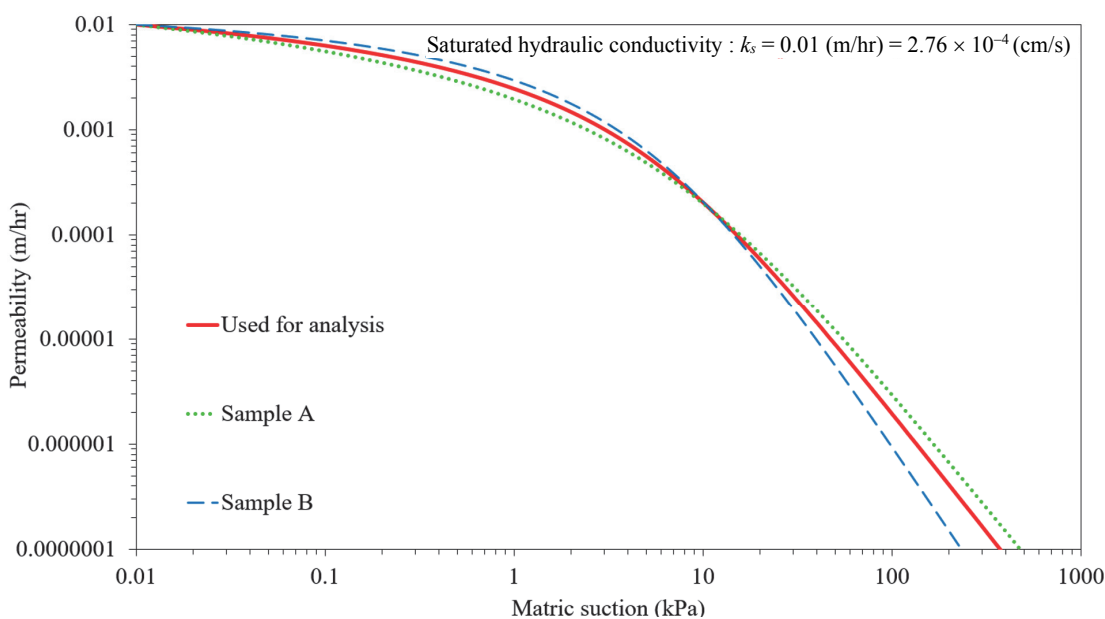


Fig. 9 Hydraulic conductivity function curves of colluvium

Using these settings, hydrological responses are obtained by SEEP/W. The results are used in SLOPE/W to determine the stability of the corresponding slope when there is infiltration by rainfall (Cai *et al.* 2004). In SLOPE/W, the extended Mohr–Coulomb failure criterion is used to calculate the shear strength of unsaturated soil Eq. (4) (Fredlund *et al.* 1978).

$$\tau = c' + (\sigma_n - u_a) \tan \phi' + (u_a - u_w) \tan \phi^b \quad (4)$$

where τ is the shear strength of the soil; c' and ϕ' respectively represent the effective cohesion and friction angles; σ_n is the effective normal stress on the failure plane and ϕ^b represents the increase in the friction angle due to the increase in shear strength

that is a result of matric suction.

4.2 Numerical Model

The analysis uses the failure mechanism for the section in the middle of the collapsing area to represent the mechanism for the entire slope. Accordingly, section A-A' (Fig. 10) is utilized for the numerical model (Fig. 11). The properties of the soil and the information regarding groundwater within the slope were attained from in-situ and laboratory tests during the site investigation by Land Engineering Consultant Co. Ltd. The locations of boreholes are shown in Fig. 10, and the detailed material properties are listed in Table 2.

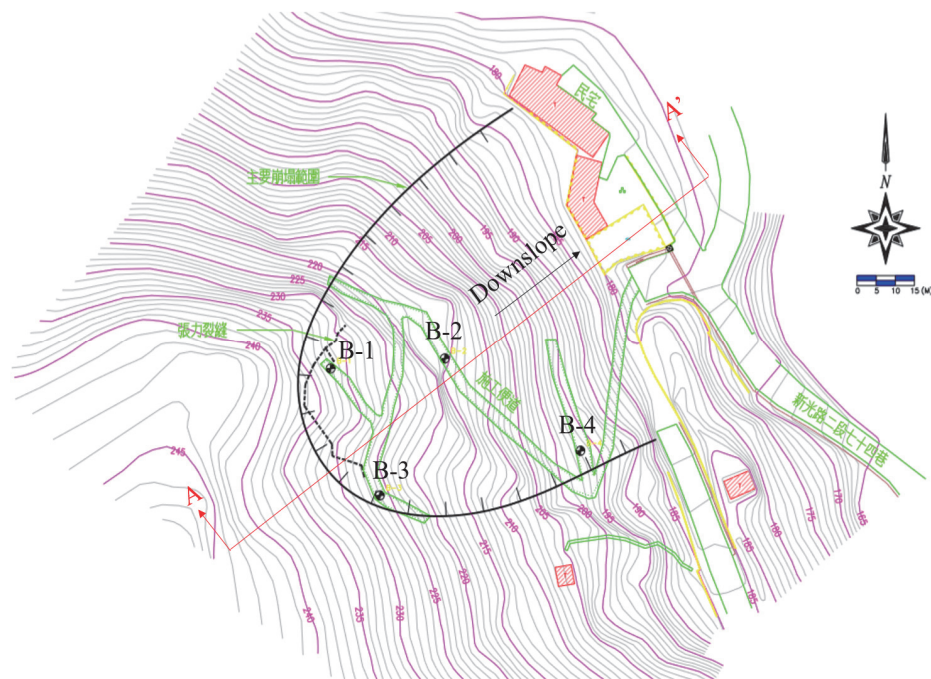


Fig. 10 Locations of boreholes and the section used in the numerical model (Land Engineering Consultants Co., Ltd. 2008)

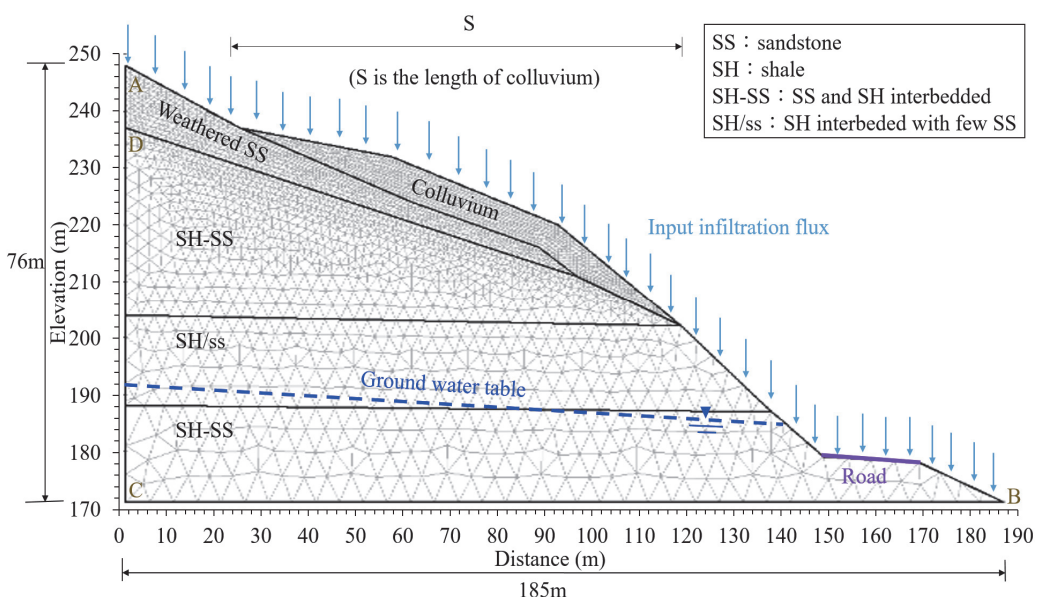


Fig. 11 Numerical model and boundary condition

Table 2 Material properties

	γ_{unsat} (kN/m ³)	γ_{sat} (kN/m ³)	Cohesion, c' (kPa) ²	Friction angle, ϕ' (°) ²	Saturated hydraulic conductivity, k_s (cm/s) ¹
Colluvial soil	19.5	20.1	6	27	2.76×10^{-4}
Weathered SS	24.6	25.4	679	36	1×10^{-8}
Sandstone and shale interbedded (SH-SS)	24.2	24.9	467	31.5	2×10^{-10}
Shale interbedded with few sandstone (SH/ss)	23.8	24.9	306	30	1×10^{-11}

¹ Yang et al. (2016)² Land Engineering Consultants Co., Ltd. (2008)

The geometry of the slope is constructed based on the topographic maps and the soil profiles are interpolated from boreholes (Land Engineering Consultants Co., Ltd. 2008). Figure 11 shows the cross-section of the slope. The average slope angle of the slope is 22°. The upper layer of the slope is colluvial soil that is 1 to 8 meters deep. Below the colluvium, there is weathered sandstone, sandstone-shale interbedded layer (SH-SS) and shale interbedded with some sandstone (SH/ss).

The height of the section is approximately 76 m, and the width is about 185 m. As shown in Fig. 11, the numerical model is composed of triangular elemental meshes. Elemental meshes of different densities are used to ensure accurate analysis and to reduce the computational time. Colluvium is the most susceptible part of the whole slope to variations in moisture under infiltration. Fine elemental meshes are used for the colluvium, but thick element meshes are used for the rock layers.

4.3 Boundary Conditions

The two lateral ends are set to be constant head boundaries in accordance with the groundwater table initially. During the analysis, downward vertical flux is utilized on the surface of the slope to stimulate infiltration. To elaborate, the input values of downward vertical flux are obtained from the hourly actual rainfall data. Nevertheless, evaporation, prescribed in upward vertical flux, is not considered during rainfall due to high humidity. Owing to low hydraulic conductivities of rocks, boundaries BC and CD were set to be total flux $Q = 0$ m³/hr. In addition, the boundary AD for weathered sandstone was seepage boundary to enable water flow (Fig. 11).

4.4 Model Parameters

Table 2 lists the parameters for the analysis. The soil properties are derived from the results of in-situ and laboratory tests from the site investigation (Land Engineering Consultants Co., Ltd. 2008). This collapse required an urgent remediation program in 2008, so there was not enough time to comprehensively figure out the failure mechanism for the case then. Therefore, soil parameters had not been completely derived at that stage. Another study used the case around the Taipei Maokong Gondola system, which is also situated in the Wenshan district of Taipei (Yang et al. 2016). On account of similar rock formation according to boreholes, it was cited to assess some hydraulic properties for this study. The saturated hydraulic conductivity of colluvium in the case (Yang et al. 2016) is adopted, shown in Table 2. In that case, the upper layer of the slope is composed of colluvium with depth from 2 to 6 m. Saturated vertical hydraulic conductivity

was determined from the field permeability test at the depth of 0.1 ~ 0.5 m by using the Guelph permeameter.

Colluvium is the most important part of the slope during rainfall infiltration. Consequently, the plate pressure test was conducted on the colluvium to ensure the accuracy of the analysis. Unsaturated seepage flow has a limited effect on rock layers because of their relatively low permeability so the rock layers are simplified into two types: SH-SS and SH/ss.

4.5 Simulation of Initial Pore Water Pressure

Since the initial groundwater table was at 25 to 45 m below the bottom of the colluvium, the pore water pressure of colluvium was -450 to -250 kPa based on the groundwater table. Nevertheless, the field suction ranges from 50 to 80 kPa at depths from 0.3 m to 1.5 m. These values were measured within the colluvium in December 2008 (Yang et al. 2016). However, the slope collapsed in September, which was the typhoon season. Thus, the field suction ought to be below the measured value above.

The approach to simulate antecedent hydrological conditions for the subsequent hydrological events has been described by Blake et al. (2003), Oh and Lu (2015), and Qi and Vanapalli (2015). The initial pore water pressure was simulated by conducting a transient seepage analysis. A small flux was specified on the surface of the slope for a long period of time until the pore water pressure reached steady state. Ultimately, the initial pore water pressure within the colluvium was -60 to -10 kPa (Fig. 12 and Fig. 13).

5. RESULTS AND DISCUSSIONS

When the initial pore water pressure had been simulated, the hourly actual rainfall data for Typhoon Jangmi was used as the input for the downward vertical flux.

5.1 Failure Mechanism and Factor of Safety

A comparison of the topographical maps before and after the collapse reveals that the primary failure mechanism for this case is a shallow collapse, shown in Fig. 14(a). Figure 14(b) shows that the critical sliding block is in the lower part of the colluvium. After the critical sliding block slides, the critical sliding block is removed in Fig. 14(c) (the purple line). By the comparison of the purple (the topography after the critical sliding block slides) and the red line (the topography after the failure of the slope). It is expected that after the initial slide the upper part of the slope (the area with slashes) became unstable and slid down progressively as displayed in Fig. 14(c).

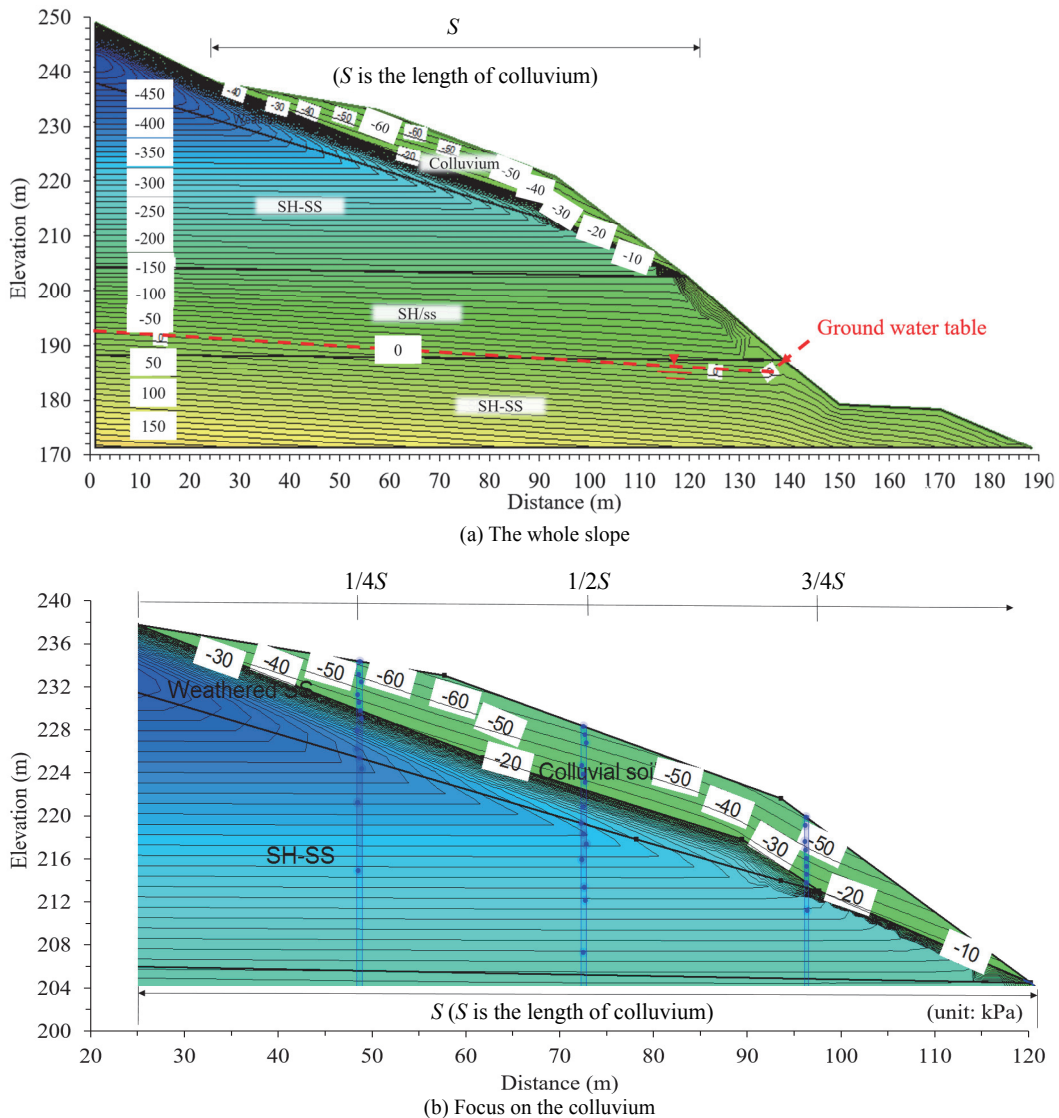


Fig. 12 Contour for the initial pore water pressure (Duration = 0hr, FS = 1.321)

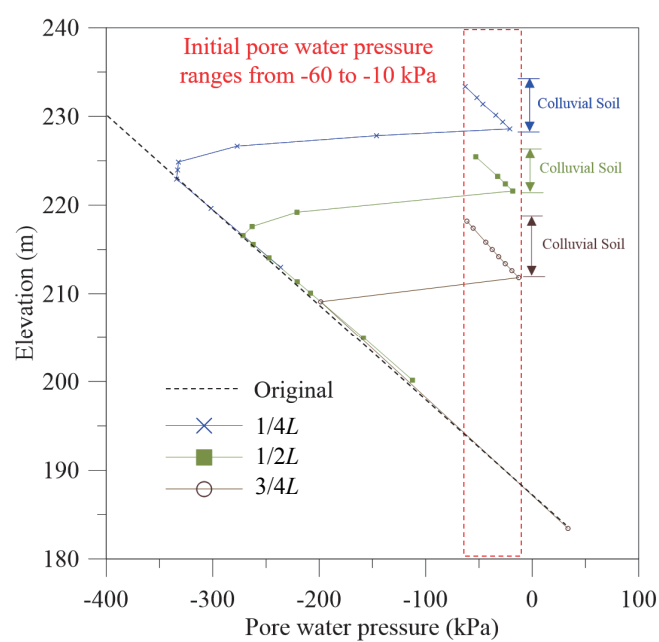


Fig. 13 Initial pore water pressure

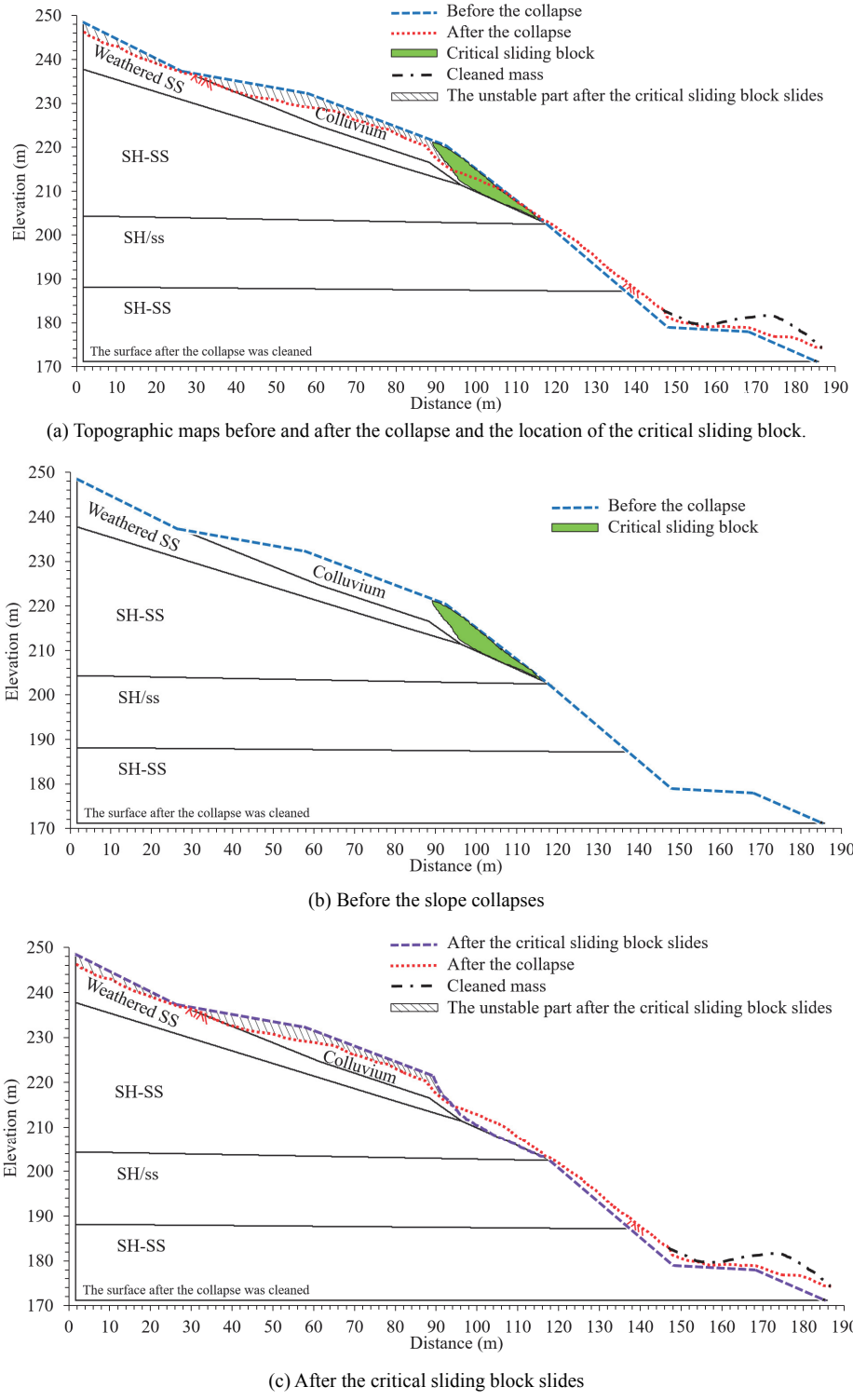


Fig. 14 Topographic maps

Overall, the factor of safety decreases when the infiltration increases. During the beginning of the rainfall for 12 hr, the factor of safety decreases with the heavy rainfall. However, from 12 hr to 24 hr, the amount of rainfall becomes light. Because the thickness of the colluvium is thin, the water flows away and dissipates easily. Hence, the value of FS increases. Then, precipitation increases after 24 hr. Consequently, the factor of safety decreases and is about 1.0 at 30 hr (Fig. 15), which is consistent with the statements of residents.

5.2 Hydrological Responses and Critical Volumetric Water Content

Figure 17 depicts the variation in the pore water pressure for three sections (Fig. 16) within the critical sliding block during infiltration. Initially, the pore water pressure for section 1/4L is -60 to -10 kPa, for section 1/2L is -40 to -10 kPa, and for section 3/4L is -30 to -10 kPa. After 30 hours of rainfall, the pore water pressure for section 1/4L is -40 to 20 kPa, for section 1/2L is 0 to 40 kPa, and for section 3/4L is 0 to 25 kPa.

Sections of $1/2L$ and $3/4L$ are fully saturated. The result indicates the complete loss of matric suction and the development of positive pore water pressure in these two sections, as the slope collapses. At this time, the critical volumetric water content is equal to the saturated volumetric water content (Fig. 18). As a

result, the primary failure mechanism for this slope is the development of the advancing wetting front. Fig. 17 shows that when the slope fails, the depth of the rainfall-induced wetting front is greater than 2 m.

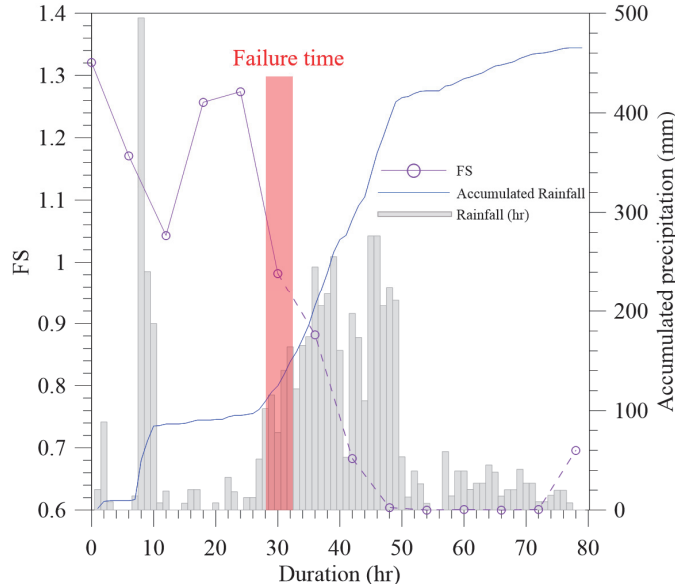
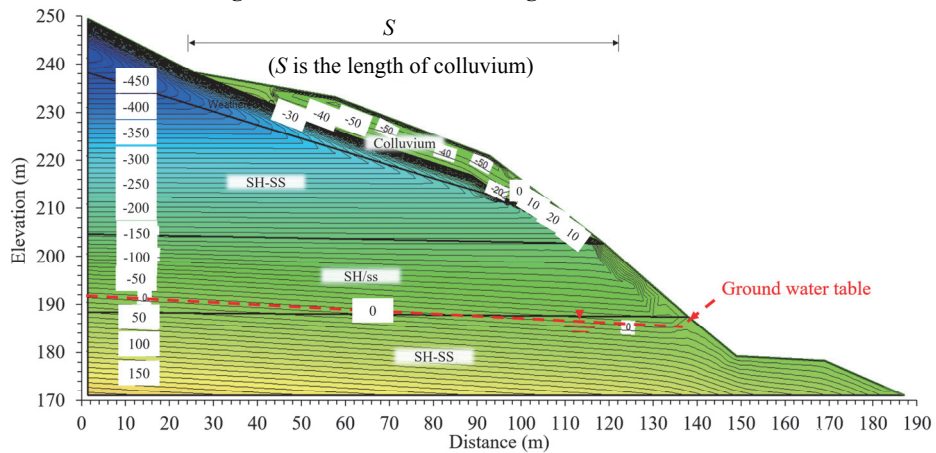


Fig. 15 Variation of FS during rainfall infiltration



(a) The whole slope

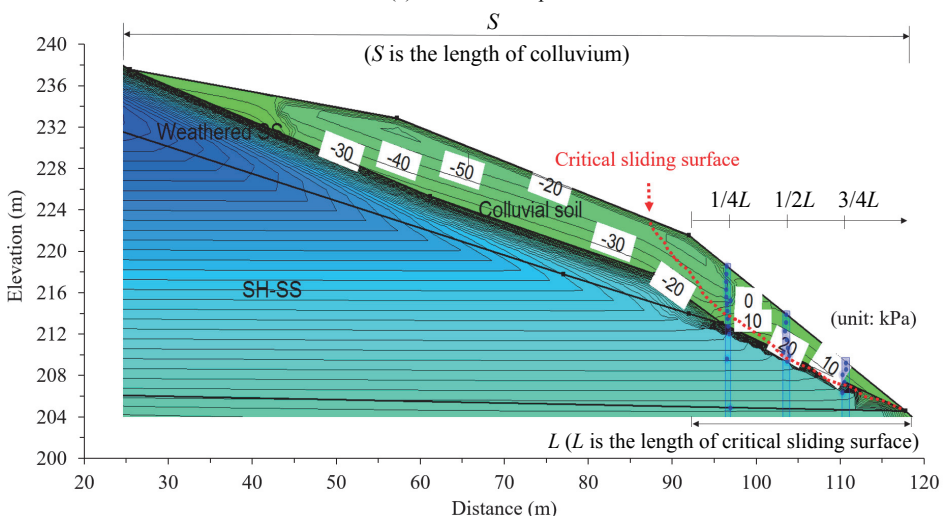


Fig. 16 Pore water pressure (kPa) contours. (Duration: 30hr, FS = 0.98)

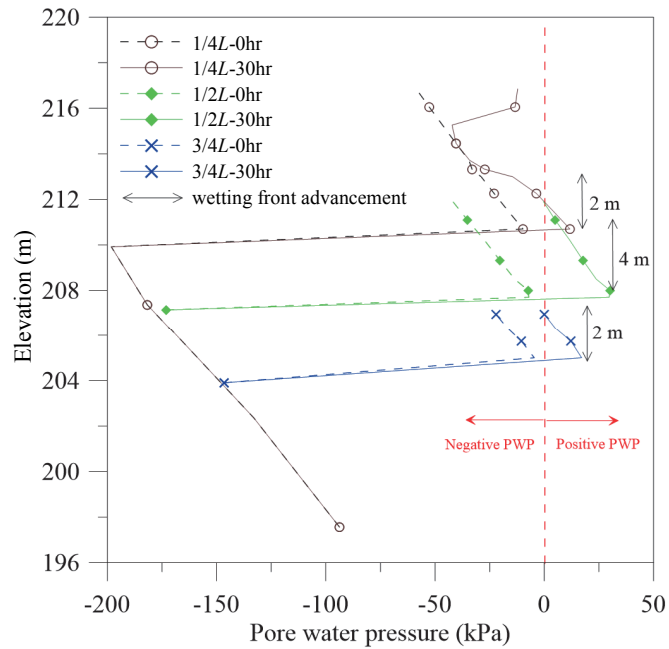


Fig. 17 Variation of pore water pressure during rainfall infiltration (Duration: 30hr, FS = 0.98)

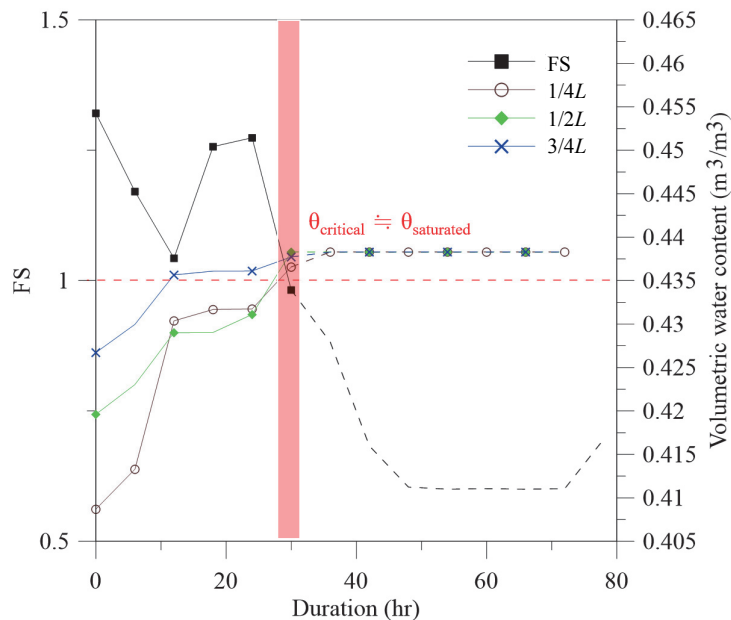


Fig. 18 Variation of FS and critical volumetric water content during rainfall

The thickness of the colluvium is non-uniform in this case. Although sections of $1/2L$ and $3/4L$ are fully saturated, section $1/4L$ is only partially saturated when the failure occurs (Fig. 17). Under the influence of gravity and because of the path of infiltration, water accumulates in the lower part of the colluvium. The critical sliding block is located in the lower part of the colluvium, which is the most sensitive portion of the entire slope subject to the rainfall infiltration. The groundwater table for this slope is also located tens of meters below the bottom of the colluvium after 30 hours of rainfall, shown in Fig. 16. Therefore, the groundwater table does not vary obviously during rainfall.

6. SUMMARY AND CONCLUSIONS

This paper presents a numerical analysis for a case study. The numerical software, Geo-Studio, is used to determine the failure mechanism and the hydrological responses for an unsaturated slope that is subject to infiltration by rainfall. The conclusions drawn from the results in this study are as follows.

1. The primary failure mechanism is a shallow collapse in this case. In addition, topographic maps reveal that the failure of the slope was progressive. To elaborate, the critical sliding block on the toe of the colluvium slides first, leading to the resistant force on the remainder of the slope decreases. Accordingly, the part above the critical sliding block for the

- slope collapses.
2. The primary failure mechanism for the unsaturated slope is the development of rainfall-induced wetting front during infiltration. As the soil became saturated under rainfall infiltration, the value of pore water pressure in the soil changes from negative to positive. Therefore, the matric suction of the soil is lost, causing a decrease in the shear strength of the soil. Hence, the factor of safety (FS) decreases.
 3. As the thickness of colluvium is uniform, the rainfall-induced wetting front develops along the surface of the slope under infiltration. Nevertheless, the thickness of the colluvium is non-uniform in this case. Because of various thickness, the wetting front develops differently for the same amount of rainfall. In this study, the toe is thinner than the head of the colluvium. Consequently, the path of infiltration is the shortest at the toe of the colluvium. Additionally, water also accumulates in the toe of the slope under the influence of gravity. That is to say, the toe of the colluvium ($3/4L$) is the most sensitive part of the whole slope subject to the rainfall infiltration.
 4. The critical volumetric water content incorporating the concepts of infiltration and mechanics is an important indicator of the landslide. Based on the results of the analysis, the critical volumetric water content is nearly equal to the saturated volumetric water content. This phenomenon indicates that the monitoring of the volumetric water content in the field can be an approach for the early warning system to predict the occurrence of landslides. It is necessary to understand the failure mechanism of the slope beforehand. As the thickness of the colluvium is uniform, the rainfall-induced wetting front develops along the surface of the slope under infiltration. Hence the volumetric water content for each section of the slope reaches the critical value simultaneously. Accordingly, in that condition, every section of the colluvium can be the appropriate place to set the monitoring system. Nonetheless, when the thickness of the colluvium is non-uniform, the development of rainfall-induced wetting front is not along the surface of the slope during rainfall. In this case, the lower part of the colluvium is the thinnest and it locates above the rock directly. Hence, water accumulates in this part easily. It is the most sensitive during rainfall, and the volumetric water content of this part reaches the critical value the earliest of the whole slope. As a result, it is recommended to set sensors for volumetric water content in the toe of the colluvium in this case. However, the appropriate place for each case to set the monitoring system should be decided by the real condition.
 5. This case is a shallow slope failure. Therefore, the slope surface protections are recommended for remediation measures in order to reduce infiltration and enhance the stability of the slope.

ACKNOWLEDGMENTS

The study is financially supported by the Ministry of Science and Technology (MOST). The authors would like to thank Land Engineering Consultants for providing data for the case and the Department of Materials Science and Engineering at National Taiwan University of Science and Technology for providing the D2 Phaser X-Ray Diffractometer for this study.

REFERENCES

- Blake, J.R., Renaud, J.P., Anderson, M.G., and Hencher, S.R. (2003). "Prediction of rainfall-induced transient water pressure head behind a retaining wall using a high-resolution finite element model." *Computers and Geotechnics*, **30**(6), 431-442.
[https://doi.org/10.1016/S0266-352X\(03\)00055-7](https://doi.org/10.1016/S0266-352X(03)00055-7)
- Cai, F. and Ugai, K. (2004). "Numerical analysis of rainfall effects on slope stability." *International Journal of Geomechanics*, ASCE, **4**(2), 69-78.
[https://doi.org/10.1061/\(ASCE\)1532-3641\(2004\)4:2\(69\)](https://doi.org/10.1061/(ASCE)1532-3641(2004)4:2(69))
- Chen, R.H., Kuo, K.J., and Chien, W.N. (2012). "Failure mechanism of granular soil slopes under high intensity rainfalls." *Journal of GeoEngineering*, TGS, **7**(1), 21-31.
[https://doi.org/10.6310/jog.2012.7\(1\).3](https://doi.org/10.6310/jog.2012.7(1).3)
- Cho, S.E. (2014). "Probabilistic stability analysis of rainfall-induced landslides considering spatial variability of permeability." *Engineering Geology*, **171**, 11-20.
<https://doi.org/10.1016/j.enggeo.2013.12.015>
- Cho, S.E. (2016). "Stability analysis of unsaturated soil slopes considering water-air flow caused by rainfall infiltration." *Engineering Geology*, **211**, 184-197.
<https://doi.org/10.1016/j.enggeo.2016.07.008>
- Chung, M.C., Chen, C.H., Lee, C.F., Huang, W.K., and Tan, C.H. (2018). "Failure impact assessment for large-scale landslides located near human settlement: case study in southern Taiwan." *Sustainability*, **10**, 1491.
<https://doi.org/10.3390/su10051491>
- Chung, M.C., Chen, C.H., Tai, T.L., and Chen, M.M. (2018). "Failure mechanism analysis considers the hydrological and seismic conditions at Chashan site in central Taiwan." *Geo-information for Disaster Management (Gi4DM)*, XLII-3/W4, 159-164.
- Collins, B.D. and Znidarcic, D. (2004). "Stability analyses of rainfall induced landslides." *Journal of Geotechnical and Geoenvironmental Engineering*, ASCE, **130** (4), 362-372.
[https://doi.org/10.1061/\(ASCE\)1090-0241\(2004\)130:4\(362\)](https://doi.org/10.1061/(ASCE)1090-0241(2004)130:4(362))
- Fredlund, D.G., Morgenstern, N.R., and Widger, R.A. (1978). "The shear strength of unsaturated soils", *Canadian Geotechnical Journal*, **15**(3), 313-321.
<https://doi.org/10.1139/t78-029>
- Gerscovich, D.M.S., Vargas, E.A., de Campos, T.M.P. (2006). "On the evaluation of unsaturated flow in a natural slope in Rio de Janeiro, Brazil." *Engineering Geology*, **88** (1-2), 23-40. <https://doi.org/10.1016/j.enggeo.2006.07.008>
- Gui, M.W. and Wu, Y.M. (2014). "Failure of soil under water infiltration condition." *Engineering Geology*, **181**, 124-141.
<https://doi.org/10.1016/j.enggeo.2014.07.005>
- Huang, C.-C. and Lo, C.-L. (2013). "Simulation of subsurface flows associated with rainfall-induced shallow slope failures." *Journal of GeoEngineering*, TGS, **8**(3), 101-111.
[https://doi.org/10.6310/jog.2013.8\(3\).4](https://doi.org/10.6310/jog.2013.8(3).4)
- Jeng, C.J. and Sue, D.Z. (2013). "Characteristics of ground motion on colluviums slope induced by heavy rainfall." *The 18th International Conference on Soil Mechanics and Geotechnical Engineering*, Paris, Technical Committee, **208**, 2189-2192.
- Kim, J., Jeong, S., Park, S., and Sharma, J. (2004). "Influence of rainfall-induced wetting on the stability of slopes in weathered soils." *Engineering Geology*, **75**(3-4), 251-262.
<https://doi.org/10.1016/j.enggeo.2004.06.017>
- Land Engineering Consultants Co., Ltd. (2008). *The Geological*

- Survey for the Repair Project in Wenshan District of Taipei* (in Chinese).
- Lee, D.H., Lai M.H., Wu, J.H., Chi, Y.Y., Ko, W.T., and Lee, B.L. (2013). "Slope management criteria for Alishan highway based on database of heavy rainfall-induced slope failures." *Engineering Geology*, **162**, 97-107.
<https://doi.org/10.1016/j.enggeo.2013.04.012>
- Lee, J.H. and Park, H.J. (2016). "Assessment of shallow landslide susceptibility using the transient infiltration flow model and GIS-based probabilistic approach." *Landslides*, **13**, 885-903. <https://doi.org/10.1007/s10346-015-0646-6>
- Lin, H.D., Kung, J.H.S., Wang, C.C., Liao, C.Y., and Tsai, M.F. (2010). "Stability analysis of unsaturated soil slope subjected to rainfall infiltration.", Keynote Lecture, *The 4th Japan-Taiwan Joint Workshop on Geotechnical Hazards from Large Earthquakes and Heavy Rainfalls*, 13-29, Sendai, Japan.
- Lin, H.D., Huang, J.R., Wang, W.C., and Chen, C.W. (2018). "Analysis of an unsaturated slope failure due to rainfall infiltration." *The Eighth Japan-Taiwan Joint Workshop on Geotechnical Hazards from Large Earthquakes and Heavy Rainfalls, Session B: Landslides and Slope Failure*, **II**, pp. 23-24, October 24-26, Uji, Kyoto, Japan.
- Lo, C.M., Wei, L.W., Hsiao, C.Y., Lin, Y.H., Cheng, C.T., and Lin, M.L. (2011). "A kinematic model of the Hsiaolin landslide calibrated to the landslide deposition pattern." *Proceedings of the Second World Landslide Forum*, Rome, 3-7.
<https://doi.org/10.1016/j.enggeo.2011.07.002>
- Montoya-Domínguez, J.D., García-Aristizábal, E.F., and Vega-Posada, C.A. (2016). "Effect of rainfall infiltration on the hydraulic response and failure mechanisms of sandy slope models." *Revista Facultad de Ingeniería Journal*, **25**(43), 97-109.
- Oh, S. and Lu, N. (2015). "Slope stability analysis under unsaturated conditions: case studies of rainfall-induced failure of cut slopes." *Engineering Geology*, **184**, 96-103.
<https://doi.org/10.1016/j.enggeo.2014.11.007>
- Qi, S. and Vanapalli, S.K. (2015). "Hydro-mechanical coupling effect on surficial layer stability of unsaturated expansive soil slopes." *Computers and Geotechnics*, **70**, 68-82.
<https://doi.org/10.1016/j.compgeo.2015.07.006>
- Richards, L.A. (1931). "Capillary conduction of liquids through porous mediums." *Physics*, **1**, 318-333.
<https://doi.org/10.1063/1.1745010>
- Shou, K.J., Wu, C.C., and Lin, J.F. (2018). "Predictive analysis of landslide susceptibility under climate change condition- a study of the Ai-Liao watershed in southern Taiwan." *Journal of GeoEngineering*, TGS, **13**(1), 13-27.
[https://doi.org/10.6310/jog.201803_13\(1\).2](https://doi.org/10.6310/jog.201803_13(1).2)
- Urciuoli, G., Pirone, M., Comegna, L., and Picarelli, L. (2016). "Long-term investigations on the pore pressure regime in saturated and unsaturated sloping soils." *Engineering Geology*, **212**, 98-119.
<https://doi.org/10.1016/j.enggeo.2016.07.018>
- Van Genuchten, M.T. (1980). "A closed form equation for predicting the hydraulic conductivity of unsaturated soils." *Soil Science Society of America Journal*, **44**(5), 892-898.
<https://doi.org/10.2136/sssaj1980.03615995004400050002x>
- Wu, T., Shih, H.J., Li, H.C., Su, Y.F., and Chen, Y.M. (2016). "Landslide impact assessment using projection rainfall data from climate change scenario." *Terrestrial, Atmospheric and Oceanic Sciences*, **27**(5), 729-740.
<https://doi.org/10.3319/TAO.2016.07.18.03>
- Yang, S.R., Lin, H.D., Kung, J.H.S., and Liao, J.Y. (2008). "Shear wave velocity and suction of unsaturated soil using bender element and filter paper method." *Journal of GeoEngineering*, TGS, **3**(2), 67-74.
[https://doi.org/10.6310/jog.2008.3\(2\).4](https://doi.org/10.6310/jog.2008.3(2).4)
- Yang, K.H., Uzuoka, R., Thuo, J.N., Lin, G.L., and Nakai, Y. (2016). "Coupled hydro-mechanical analysis of two unstable unsaturated slopes subject to rainfall infiltration." *Engineering Geology*, **216**, 13-30.
<https://doi.org/10.1016/j.enggeo.2016.11.006>